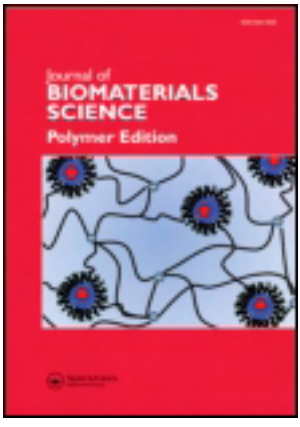

Journal of Biomaterials Science, Polymer Edition
Publication details, including instructions for authors and subscription information:
http://www.tandfonline.com/loi/tbsp20

Mechanical properties of a self-assembling oligopeptide matrix

Erasmo J. Leon [a], Neeta Verma [b], Shuguang Zhang [c], Douglas A. Lauffenburger [d] & Roger D. Kamm [e]

[a] Center for Biomedical Engineering, Massachusetts Institute of Technology, Canbridge, MA 02139, USA

[b] Center for Biomedical Engineering, Massachusetts Institute of Technology, Canbridge, MA 02139, USA

[c] Center for Biomedical Engineering, Massachusetts Institute of Technology, Canbridge, MA 02139, USA

[d] Center for Biomedical Engineering, Massachusetts Institute of Technology, Canbridge, MA 02139, USA

[e] Center for Biomedical Engineering, Massachusetts Institute of Technology, Canbridge, MA 02139, USA

Version of record first published: 02 Apr 2012.

J. Biomater. Sci. Polymer Edn, Vol. 9, No. 3, pp. 297–312 (1998)

Mechanical properties of a self-assembling oligopeptide matrix

ERASMO J. LEON, NEETA VERMA, SHUGUANG ZHANG, DOUGLAS A. LAUFFENBURGER and ROGER D. KAMM*

Center for Biomedical Engineering, Massachusetts Institute of Technology, Canbridge, MA 02139, USA

Received 3 June 1997; accepted 6 October 1997

Abstract—We have begun studies of a novel type of biomaterial derived from a recently-discovered class of ionic self-complementary oligopeptides. These short peptides (typically 8, 16, 24, or 32 amino acid residues with internally-repeating sequences) self-assemble in aqueous salt solution into three-dimensional matrices capable of favorable interactions with cells, and offer promise for useful bioengineering design based on rational changes in sequence. In this paper we present preliminary results on mechanical properties, combining experimental and theoretical approaches, of one particular example of these peptide materials, EFK8. The static elastic modulus was measured using an apparatus designed to allow sample fabrication and mechanical testing in the same system with the sample in aqueous solution. The material microstructure was examined by SEM and the measurements interpreted with the aid of a model for cellular solids. Values for the elastic modulus increased from 1.59 ± 0.06 to 14.7 ± 1.0 kPa for peptide concentrations increasing from 2.7 to 10 mg ml^{-1}. SEM photographs showed the microstructure to consist of a relatively homogeneous lattice with fiber thickness of $10 - 30$ nm independent of peptide concentration, but with fiber density increasing with peptide concentration. This behavior is consistent with scaling predictions from the cellular solids model and yields an estimate for the individual fiber elastic modulus in the range of 1–20 MPa. We therefore have provided some initial physical principles for guiding improvement of the mechanical properties of these new materials.

Key words: Biomaterial; self-assembling peptides; elastic modulus; model; tensile test; microstructure.

INTRODUCTION

It is widely recognized that the current repertoire of biomaterials will not be adequate for the vast range of applications in drug delivery, artificial organs, and tissue engineering technologies (e.g. [1–4]). Issues that must be resolved satisfactorily for development of new biomaterials suitable for particular applications include: (a) capability for providing molecularly-specific interactions with cells; (b) capability for minimization of immune and inflammatory responses; (c) capability for controlled

*To whom correspondence should be addressed. E-mail: rdkamm@mit.edu

degradation into harmless constituent products on appropriate time scales; (d) capability for offering proper permeabilities to diffusible nutrients, regulatory factors, and cell products; (e) capability for exhibiting necessary mechanical properties; (f) capability for reproducible GMP synthesis and fabrication; and, (g) capability for flexibility in molecular-level design. While diverse approaches to development of new materials are being pursued energetically in numerous laboratories, it is highly improbable that a single class of materials will resolve all these issues optimally for the entire range of applications. Thus, innovative directions with the potential for success in even a subset of applications need to continue to be strongly encouraged.

Recently, a new class of ionic, self-complementary oligopeptides has been discovered [5] and its potential value as a biomaterial is currently being explored. These short (8-, 16-, 24-, and 32-amino acid residue monomers) oligopeptides consist of regular repeats of alternating ionic hydrophilic and hydrophobic amino acids and associate to form stable β-sheet structures in water [5, 6]. The addition of buffers containing millimolar amounts of monovalent salts results in the spontaneous assembly of the oligopeptides into a stable, macroscopic membranous matrix; this assembly is facilitated by ionic side chain interactions in addition to conventional β-sheet backbone hydrogen bonding.

This class of peptide biomaterials has several attractive features. Because they are short oligomers, they can be readily synthesized *in vitro* from entirely *de novo* design, and subsequently, purified, manipulated and modified. The twenty natural amino acids — as well as numerous 'non-natural' amino acids — potentially allow a wide range of physico-chemical properties, such as mechanical strength, permeability, and degradation rates, to be custom-generated for particular applications. Since they arise via self-assembly in aqueous salt solutions, they can be produced using fabrication processes that introduce no toxic solvents.

In terms of biologically-relevant features, the natural pore size arising in these matrices — roughly 100 nm — is appropriate for diffusive transport of regulatory molecules. Furthermore, a diverse spectrum of cells has been demonstrated to interact favorably with the materials in terms of attachment, spreading, and migration [7]. At the same time, their strongly ionic character [5, 7] minimizes their immunogenicity. In matrices for which their constituent monomers are all natural L-amino acids, their degradation will yield normal amino acids which can then be reused by the host tissue. They are resistant to heat, to many chemical denaturation agents, and to degradation by proteolytic enzymes *in vitro*, nonetheless appear to resorb *in vivo* [5, 6].

Although these peptide materials possess many desirable properties, our initial experience has shown that they are rather fragile and somewhat difficult to handle. Since problematic structural integrity could limit the range of usefulness of these materials, we are now focusing on the structural characteristics of the materials, with an aim toward developing a more fundamental understanding of those factors that influence them and to identifying methods by which materials with appropriate strength can be designed.

In this paper, we explore the mechanical properties of one particular peptide from this class, EFK8. Methods are developed for measuring the elastic modulus and fracture strength using minute specimens. The microstructure is examined by SEM

and an existing theory for cellular solids is used as one framework within which the microstructure and measurements might be related.

METHODS

Mechanical testing

To allow the testing of samples under uniaxial stress, cylindrical threads were produced. These are fabricated using the apparatus shown in Fig. 1, consisting of a micrometer-controlled translating stage with the extrusion needle attached, a syringe pump to control the flow rate of peptide solution, and a cuvette containing salt solution placed on an electronic balance. The specimen is visually recorded by means of a high resolution CCD camera (Pulnix TM-9700). Both the video signal and the signal from the electronic balance (Denver Instruments) are fed into a data acquisition system (Macintosh Power PC, Model 8500).

Cylindrical threads of peptide biomaterial are formed vertically in the cuvette which contains salt solution with density matched to that of the injected peptide to eliminate buoyancy effects. Initially a small amount of peptide is injected to produce a base that adheres to the bottom of the cuvette. The needle is then raised at a speed commensurate with the ejection flow rate to produce a cylindrical thread approximately the same diameter as the needle. The values used were 65 $\mu m\,s^{-1}$ for the needle withdrawal speed and 0.097 $mm^3\,s^{-1}$ for the flow rate.

Using this method, specimens of the type shown in Fig. 2 are readily produced. The test specimens typically had bottom and top anchors 2 mm in length and 1.6 mm in diameter. At their narrowest point, the neck had an approximate length and diameter

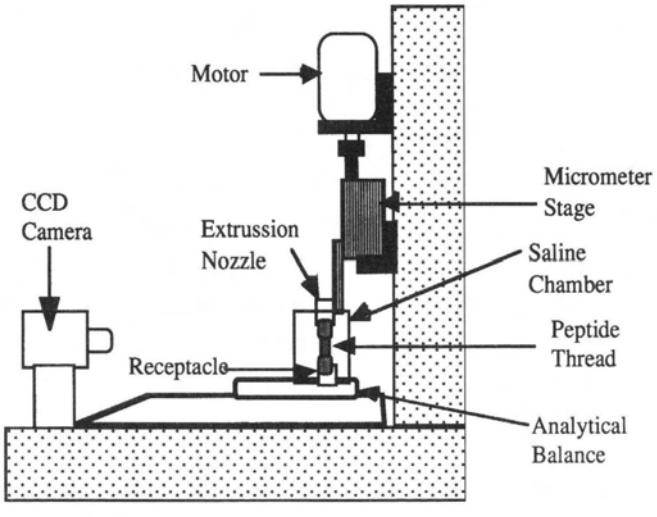

Figure 1. Schematic of tensile testing system.

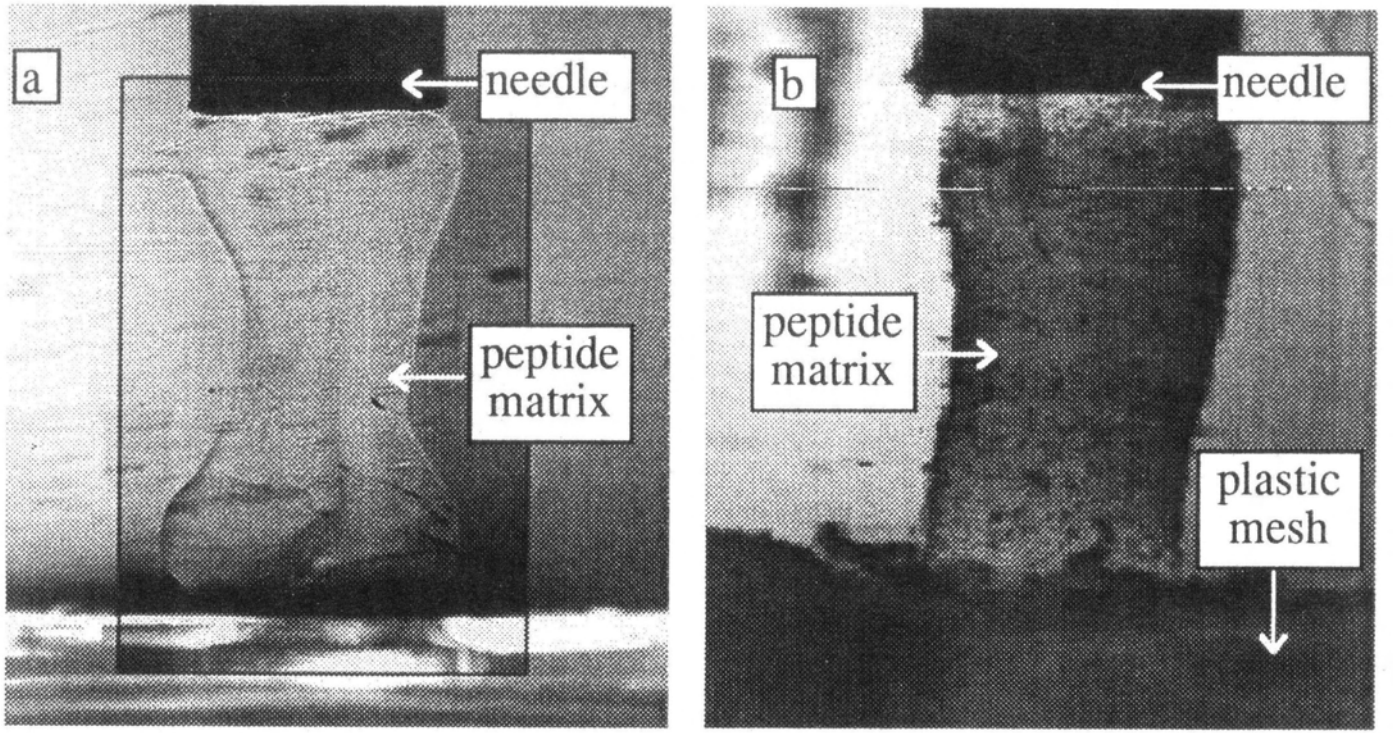

Figure 2. Photographs of tensile test specimens: (a) specimen after fabrication (shaded box shows enhanced contrast to allow observation of colorless specimen); (b) specimen anchored to plastic mesh (Congo red stain added to enhance specimen visibility).

of 8 mm and 1.4 mm, respectively. The images used to measure lengths and displacements can resolve 7.3 μm. Since the length monitored for strain measurements is approximately 0.8 mm, the uncertainty introduced in strain measurements is about 0.9% elongation compared to measured strains of up to 8%. The effect of this error can be reduced by making multiple measurements from a given test as discussed below. The balance used to measure resulting forces on the specimen has a resolution of 0.1 mg corresponding to a force of 9.8×10^{-7} N. The forces measured in the experiments ranged from 9.8×10^{-6} to 2×10^{-4} N (stresses from 6 to 127 Pa).

Once formed, the peptide biomaterial solidifies on a diffusional time scale ($\sim$ minutes for samples as shown in the figure). When solid, the specimen can be immediately subjected to mechanical tests without removal from the fabrication apparatus. Small increments (~ 0.01 mm) are made in the micrometer stage while the video and force signals are recorded. After a short transient (< 1 min) the force stabilizes and the next increment is imposed. Stress can be computed as the change from baseline force, divided by the cross-sectional area, determined from the diameter measured from the video signal. Strain in the central region (away from the ends of the specimen) can be calculated as the change in distance between two identifiable points on the surface of the peptide thread. Ultimately, the specimen fractures, usually near its midpoint (tests in which the fracture occurs near one of the ends are discarded).

Scanning electron microscopy

After self-assembly of the peptides into macroscopic matrices, we examined the detailed material structure with scanning electron microscopy (SEM). The oligopeptide matrices were prepared for SEM by incubating the matrices in 5% glutaraldehyde at 4°C for 2 h, followed by slow sequential dehydration steps in 10% increments of ethanol in PBS for 5 min each. The sample was then placed in pressurized liquid CO_2/syphon for 1 h. The sample was next sputter-coated with gold–palladium particles, mounted on a grid and examined using a JEOL JSM-6320FV field emission SEM at between 2000 and 100 000 $\times$ magnification [7].

The SEMs were analyzed to quantify the structural parameters relevant to the mechanical properties. The public domain software package, NIH Image (ver. 1.60) was used to identify the diameter of the fibers, and their junction-to-junction distance. Length measurements were corrected to account for the three-dimensionality of the structure. On the assumption that the material is isotropic (so that every orientation is equally likely), the mean length determined from the two-dimensional image was multiplied by $4/\pi$ to give the true mean length. This correction is not necessary for fiber diameters assuming them to be circular in cross-section. The mean values thus obtained were used to determine the density of the fiber matrix.

Peptide

This study concentrates on a single peptide, EFK8 (N-KFEFKFEF-C), the chemical structure of which is shown in Fig. 3. The negative and positive charged amino acids are glutamate (E) and lysine (K), respectively. The hydrophobic R-group is provided

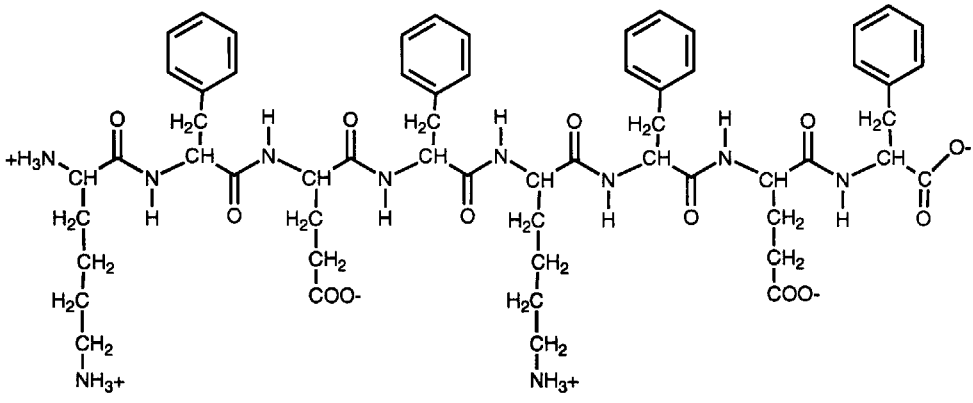

Figure 3. Molecular structure of the oligopeptide, EFK8.

by the aromatic amino acid phenylalanine (F). A molecular model of EFK8 produced with Molecules 3-D (ver. 2.1), is included in the figure. This model clearly shows the bulky hydrophobic phenylalanine R groups lying on one side of the β-sheet and the charged glutamate and lysine R groups lying on the opposite side.

EFK8 is one of the smallest peptides in the family of ionic self-complementary oligopeptide biomaterials. Presently, 8-mers are the smallest peptides that form part of this class of materials. Previous studies suggest that longer peptides are more stable than shorter ones and show greater tendency for self-assembly. However, the shortest peptides offer the advantage of lower cost, greater ease of synthesis, and higher solubility and purity. Also, shorter peptides show lesser structural and chemical complexity, which facilitate their study. Therefore, the study of small peptides provides the starting point towards greater comprehension of the self-assembling oligopeptide biomaterials and their material properties.

Cellular solids model

The theory of cellular solids relates the mechanical properties of low density cellular materials to their structural characteristics [8] and has been successfully used to characterize materials ranging from cotton to the F-actin intracellular matrix [9]. The analysis is based on the concept that the material can be thought of as being comprised of many 'unit cells', one representation of which is shown in Fig. 4. These unit cells are staggered with struts meeting at their midpoints. It should be noted that the following analysis, while developed with the structure of Fig. 4 in mind, has been shown to be applicable to a variety of fibrous materials with different microstructures. When a cellular solid is stressed under tension or compression, the fibers act like struts and beams that deform under stress as illustrated in Fig. 4b. At loads exceeding the linear–elastic regime, the struts can buckle and plastic hinges are created [8]. This leads to plastic collapse of the structure. If the constitutive material is brittle, brittle crushing or brittle fracture are the cause of collapse [8].

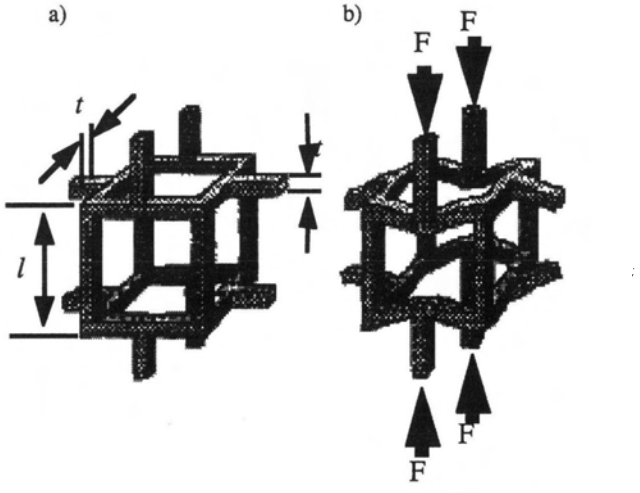

Figure 4. Unit cell model used in theoretical model of mechanical strength: (a) undeformed; and (b) loaded and deformed by element bending (adapted from Gibson and Ashby, 1988).

The unit cell model in Fig. 4 has struts or fiber elements of length l and thickness t. The relative density of the material is defined as the density of the network, ρ^*, divided by the density of the fibers ρ_s. This ratio depends on the geometry of the matrix structure. It is related to the cell dimensions t and l [8].

$$\frac{\rho^*}{\rho_s} \propto \left(\frac{t}{l}\right)^2. \tag{1}$$

Beam theory [10] gives the deflection δ of a beam of length l to a force F acting at its midpoint as

$$\delta \propto \frac{Fl^3}{E_s I}, \tag{2}$$

where E_s is the stiffness of the beam constitutive material and I is the beam's second moment of area. The moment of area for a beam of thickness t is given by

$$I \propto t^4. \tag{3}$$

The stress σ is the force per unit area, or

$$\sigma \propto \frac{F}{l^2}. \tag{4}$$

The strain is related to beam deflection δ by

$$\varepsilon \propto \frac{\delta}{l}. \tag{5}$$

Using the results from Eqs (2), (4), and (5), the network Young's modulus or elastic modulus can be expressed as

$$E^* = \frac{\sigma}{\varepsilon} = \frac{kE_s I}{l^4}, \tag{6}$$

where k is a constant of proportionality. Substituting Eqs (1) and (3) into (6) gives [8]:

$$\frac{E^*}{E_s} = k_1 \left(\frac{\rho^*}{\rho_s}\right)^2. \tag{7}$$

Data from a wide range of materials and cell geometries give a value for k_1 of approximately 1. A similar analysis for cellular materials subjected to shear stresses results in an expression for the network shear modulus G^* given by [8]:

$$\frac{G^*}{E_s} = k_2 \left(\frac{\rho^*}{\rho_s}\right)^2, \tag{8}$$

where $k_2 \sim 3/8$. If the material is linear-elastic and isotropic, elasticity theory [10] provides the following relationship

$$G = \frac{E}{2(1+\nu)}, \tag{9}$$

which, when solved for the Poisson ratio ν, gives a value of $1/3$.

Brittle materials in tension fail by propagation of cracks. The scaling analysis of this deformation mechanism is done using the results of linear elastic fracture mechanics. It relates the network fracture toughness K^* to the solid toughness K_s by

$$\frac{K^*}{K_s} = k_3 \left(\frac{\rho^*}{\rho_s}\right)^{3/2}. \tag{10}$$

Extensive data dictate the value of k_3 to be approximately 0.65 [8].

Finally, it should be noted that each of these expressions involving a density ratio (ρ^*/ρ_s) can also be expressed in terms of a concentration in the form:

$$\frac{\rho^*}{\rho_s} = \frac{k_4}{C}, \tag{11}$$

where k_4 can be taken to be a constant on the assumption that the peptide concentration within the fibers is independent of bulk concentration. Substituting Eq. (11) into (7), (8), or (10) provides a scaling relation for the dependence of elastic, shear and toughness moduli on peptide concentration.

RESULTS

Characterization of microstructure using SEM

Micrographs obtained from critical-point dried samples of EFK8 are shown in Figs 5 and 6 at 3.3 and 10.0 mg ml^{-1}, respectively. The macroscopic membrane formed by the peptides is seen to consist of a low density fibrous material At the lower magnifications, namely, 2000 and 4000 ×, the specimen has the appearance of a

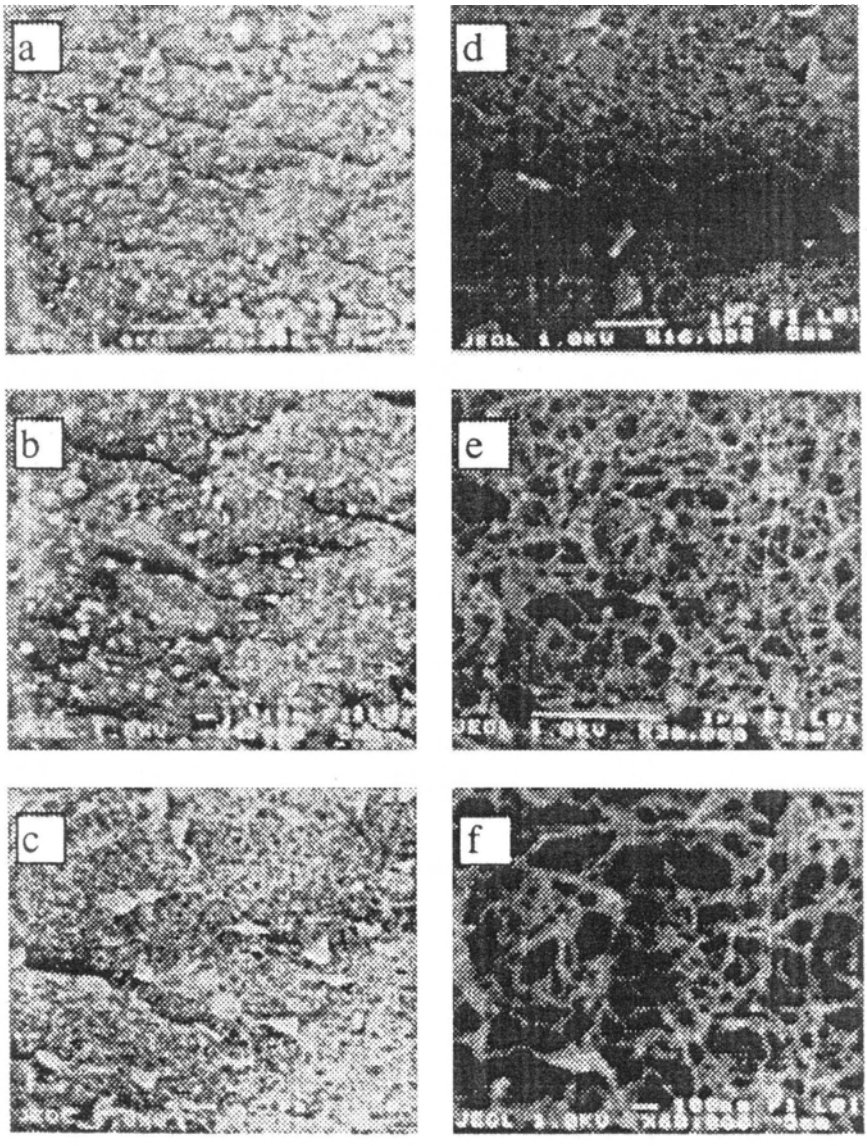

Figure 5. Scanning electron micrographs of EFK8 at 3.3 mg ml^{-1}. Magnifications of: (a) 2000; (b) 4000; (c) 8000; (d) 16 000; (e) 32 000; and (f) 60 000.

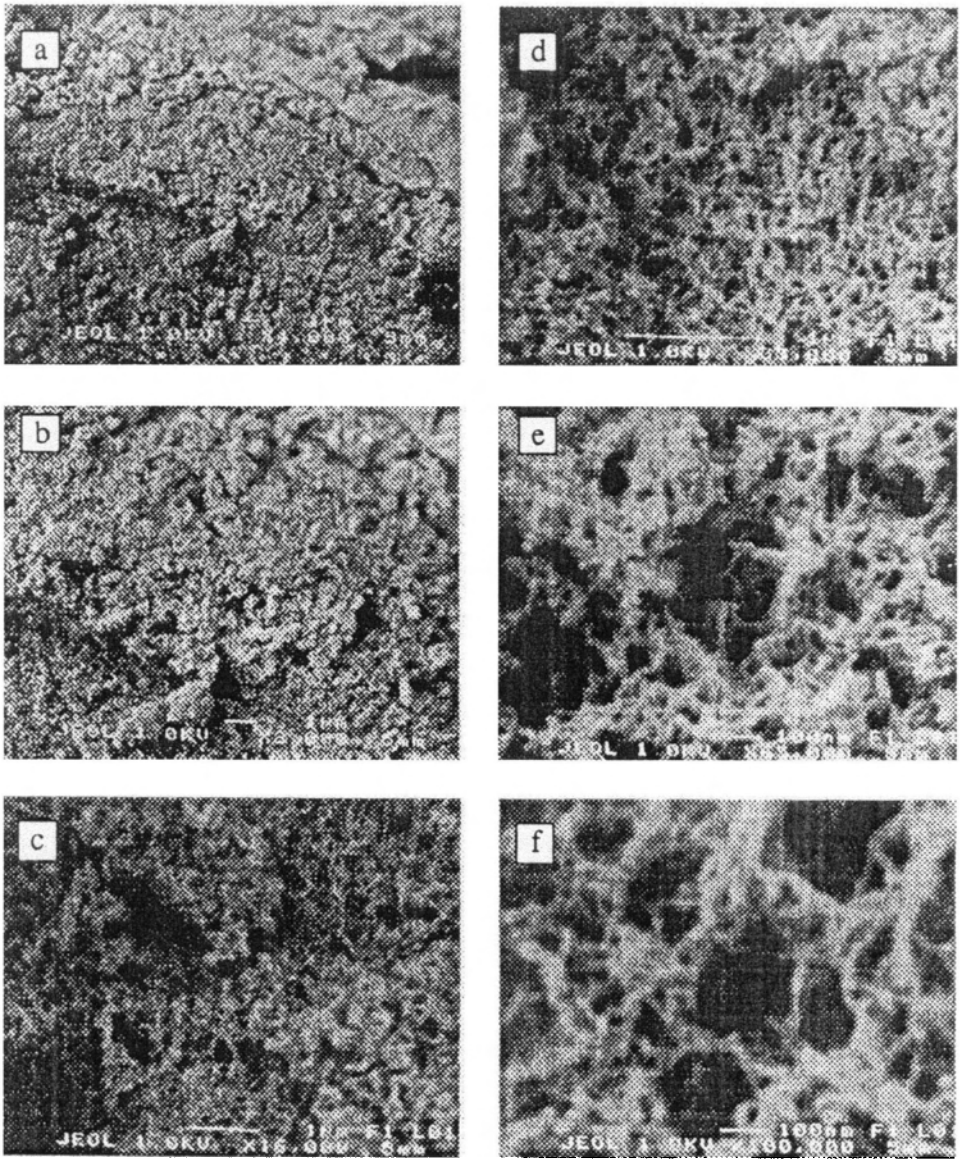

Figure 6. Scanning electron micrographs of EFK8 at 10 mg ml^{-1}. Magnifications of: (a) 4000; (b) 8000; (c) 16 000; (d) 33 000; (e) 65 000; and (f) 100 000.

continuous solid with a rough surface. At the higher magnifications of 16 000 × and 32 000 × the material's porous structure becomes discernible.

At a concentration of 3.3 mg ml^{-1}, the material can be described as a mesh of randomly interconnected fibers. These filaments are interwoven forming a macroscopic porous matrix [5, 7]. The fibers show no apparent preferred orientation, nor are there any systematic variations in fiber thickness or edge-connectivity. These fibrous networks have a fairly uniform appearance compared to those formed at higher

concentrations with fiber thicknesses 10–30 nm (after correction for the thickness of the gold coating) and distance between fiber junctions of 100–250 nm.

The high magnification micrographs of EFK8 at 10 mg ml^{-1} revealed that the detailed microstructure differs somewhat from that of the same peptide at 3.3 mg ml^{-1}. Comparison of their respective pictures clearly illustrate that the 10 mg ml^{-1} peptide dilution resulted in a denser matrix. The fibers have similar thickness (10–30 nm), however, the 10 mg ml^{-1} sample has a larger number of fibers per volume and a correspondingly shorter fiber length of 50–100 nm. Notably, the network of the 10 mg ml^{-1} sample is less uniform than that observed at 3.3 mg ml^{-1}. These inhomogeneities are especially evident in the 65 000 and 100 000 × magnifications of Fig. 6e and f, respectively.

Tensile tests

Tensile tests were performed on EFK8 specimens at concentrations of 2.7, 3.3, 5.4, and 10 mg ml^{-1}. Figure 7 illustrates the averaging method used to determine the stress–strain curve for a single experiment. Four curves are shown; the solid curves correspond to strain measurements obtained using three different paired points near the center of the specimen. The dashed curve depicts the stress–strain behavior that resulted from averaging the three individual curves.

The three curves in Fig. 8, each obtained from the averaging procedure just described, suggest that the stress–strain behavior of the peptide material at 2.7 mg ml^{-1}

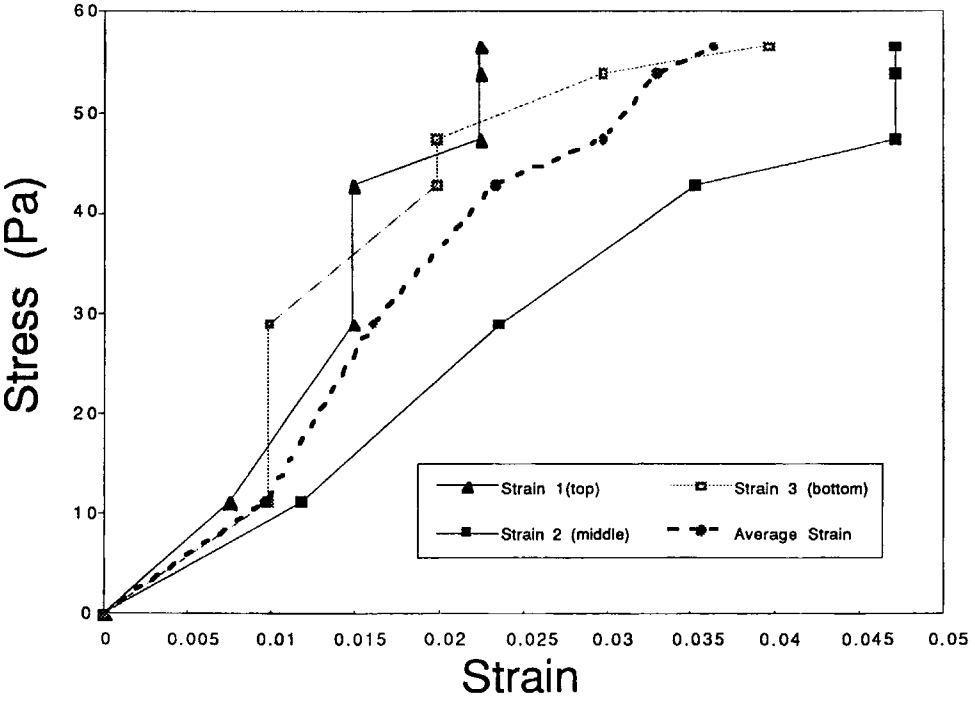

Figure 7. Averaging strain technique for stress–strain curves. Individual curves correspond to different pairs of reference points on specimen. Tensile test of EFK8 at 2.7 mg ml^{-1}.

Table 1.
Tensile tests data for EFK8

Concentration (mg ml^{-1})	Modulus (kPa)		Strength (Pa)		Max. elongation (%)	
	Range	Average	Range	Average	Range	Average
2.7	1.52 – 1.63	1.59 ($n = 3$)	44 – 57	50.5 ($n = 2$)	3.0 – 3.6	3.3 ($n = 2$)
3.3	2.67 – 3.32	2.90 ($n = 4$)	119 – 218	176.3 ($n = 4$)	4.4 – 7.8	5.9 ($n = 4$)
5.4	5.0 – 7.3	6.23 ($n = 3$)	123	123 ($n = 1$)	1.7	1.7 ($n = 1$)
10	14.0 – 15.4	14.7 ($n = 2$)	162 – 231	196.5 ($n = 2$)	1.1 – 1.3	1.2 ($n = 2$)

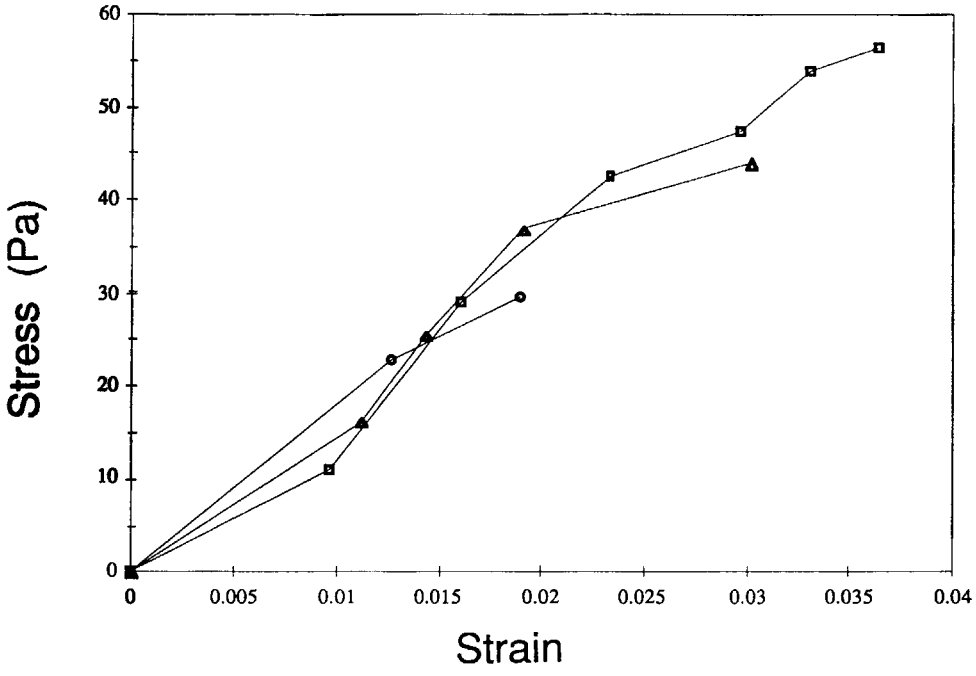

Figure 8. Tensile stress–strain curves for EFK8 at 2.7 mg ml^{-1}. Each curve is averaged as in Fig. 7.

is essentially linear all the way to fracture. The Young's modulus (values reported in Table 1 and Fig. 9) was obtained from the slope of the least squares linear regression for stress vs strain. Two of the three curves include data all the way to fracture. In both cases, fracture occurred near the middle of the specimen.

The data for all four concentrations exhibited similar linearity, although the experimental noise, primarily due to limitations imposed by the spatial resolution of the imaging set-up, cause increasing scatter at higher concentrations as the total strain before fracture decreases.

The mechanical measurements are summarized in Table 1. This table presents the elastic modulus, fracture strength, and strain to fracture at the four concentrations, presented as a range and an average. These data demonstrate a trend of increasing Young's modulus with increasing concentration. The fracture strength also exhibits

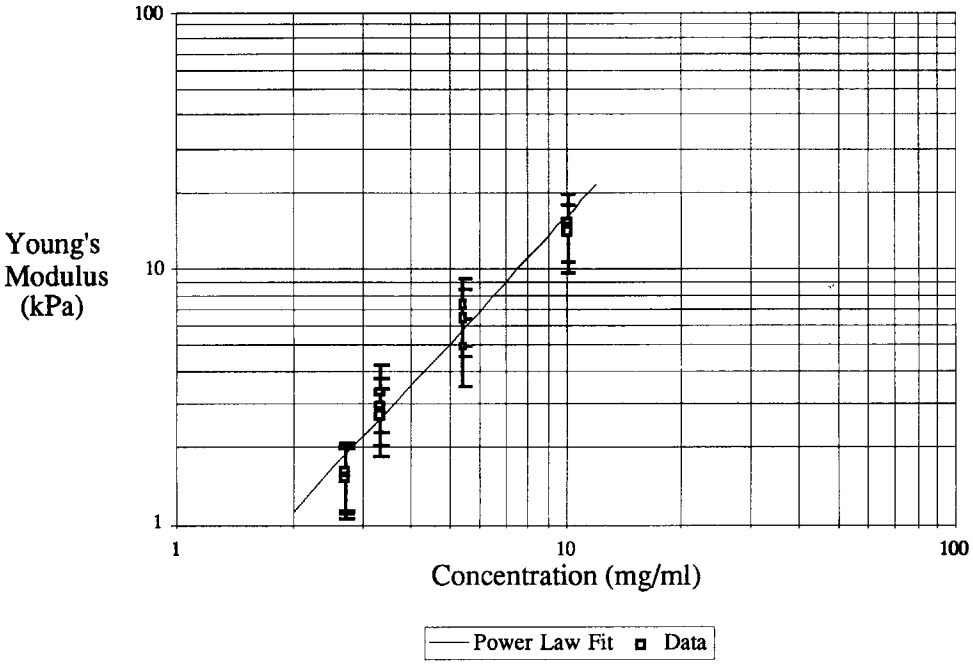

Figure 9. Dependence of Young's modulus on peptide concentration for EFK8. Solid line is best logarithmic fit to the data.

some tendency to increase with concentration although this tendency is masked by the high degree of scatter in the fracture results and the mean values are not significantly different. The elongation, however tends to decrease with increasing material concentration.

The Poisson ratio was determined from a ratio of the diametrical strain to the axial strain, measured near the midpoint of the specimen. The value determined from these measurements was 0.47 ± 0.16.

Cellular solids analysis

The cellular solid analysis suggests that the elastic or Young's modulus should vary as C^2. Although the values for elastic modulus plotted in Fig. 9 show a clear tendency to increase with increasing concentration, when the experimental data are fit to a power law relationship, the dependence of concentration is found to be somewhat weaker than predicted by the scaling analysis, satisfying

$$E^* \cong 0.36C^{1.6}, \tag{12}$$

where E^* is in kPa and C is in mg ml^{-1}. This regression line is also shown in the figure.

An estimate for the elastic modulus of the individual fibers comprising the matrix can be obtained from Eq. (7), using the value of the constant found from other studies ($k_1 \sim 1$). Using a fiber dimension in the range of 10–30 nm, the measured values of

matrix stiffness, and values for fiber length obtained by image analysis, fiber elastic modulus is estimated to be in the range 0.6–23 MPa.

DISCUSSION

Earlier studies have demonstrated that the self-complimentary ionic oligopeptides may have considerable potential for use as biomaterials in drug delivery, wound healing, and tissue regeneration [5–7]. Practical application, however, will require further investigation of key properties of the materials and their interactions with a biological environment. An initial question concerns the ability of these materials to respond in satisfactory manner to mechanical stresses likely to be imposed. Hence, the primary purpose of this study was to measure the static elastic properties of one member of this new class of peptide biomaterials and interpret these measurements with the aid of scanning electron microscopy complimented by analysis.

For the purpose of measuring the mechanical properties of these materials, it was necessary to design a new test apparatus that met several stringent requirements. Because of the high cost of synthesizing new oligopeptides, the specimen volume needed to be as small as possible. Due to the fragility of such small samples, and because of the need to maintain an aqueous environment, it was decided that fabrication and testing should be done in the same system. The use of an electronic balance in this setting simultaneously provided the required accuracy in load measurement and the capability of taring the system, including cuvette and aqueous solution, just prior to testing. In order to avoid artifacts associated with end regions, the image analysis method was selected for strain measurement. This also precluded the need for direct contact with the specimen. The main limitation of this system was the resolution of the strain measurements. Before performing the experiments it was felt that $\sim 10\ \mu$m resolution would be adequate; it was not until measurements were made with the high concentration samples that the limitations of the constrain were evident. The use of a lens with higher magnification would obviously improve the accuracy of the strain measurements.

The microstructure as seen in the SEMs consists of an isotropic lattice with fibers of nearly uniform thickness. It is interesting to note that the fiber thickness is comparable to the length of the oligopeptide molecule, suggesting a possible link. The fiber length between junctions (and therefore the pore size) is somewhat more variable, to an increasing degree as the peptide concentration is increased. These inhomogeneities may, however, have been more accentuated on the surface of the gelled thread where the SEMs were obtained. More study is needed to determine the extent to which the sample is spatially uniform. It is apparent from these results, that extrusion of the solution into the aqueous bath at these rates did not produce a preferred fiber orientation.

The elastic modulus exhibited by these preliminary measurements on EFK8 (of approximately 10 kPa at easily practicable peptide concentrations), compares favorably with that of soft tissues, for example, young male thigh and forearm skin with respective moduli of 1.99 and 1.51 kPa [11]. It is also comparable to the elastic modulus of

biomaterials considered as potential candidates for scaffolds in engineered soft tissue. Collagen sponge, for example, has an elastic modulus of 5 kPa at a concentration of 0.5–2.0%, but this can be increased to 20 kPa by cross-linking with glutaraldehyde [12, 13]. All these values, however, lie far below those used in the repair of bone or connective tissue which are in the range of 400 to 10 000 MPa [14–16].

The matrix modulus is low primarily because of the low volume fraction of the gel rather than because the individual fibers lack sufficient strength. This can be seen from a comparison of our estimate of the fiber modulus (0.6–23 MPa) to the fiber modulus for other polymers such as latex rubber and polybutadiene with moduli of 2.6 MPa and 1–50 MPa [8], respectively.

There are several approaches that could be considered to increase this material's strength and modulus. According to the scaling predictions of the cellular solids theory, the elastic modulus will increase roughly as the square of the peptide volume fraction, and the fracture strength by the 3/2 power. This suggests that one promising approach would be to investigate methods for increasing the solubility of peptide in water. Concentrations of up to 10 mg ml^{-1}, as used in the present tests, are easily achieved; higher concentrations, with EFK8 or another oligopeptide, are readily produced. The samples tested, however, exhibited a less strong dependence on concentration than predicted by the theory. One likely cause for this is the increasing degree of inhomogeneity observed as peptide concentration was increased. It remains to be seen, therefore, whether the increases suggested by the theory will actually be attainable. A second means of increasing the elastic modulus is through cross-linking, or otherwise increasing the strength of the intermolecular bonds. Cross-linking, for instance, can be accomplished by introducing multiple cysteine residues into the oligopeptide to allow for disulfide linkage via thiol groups. This approach is especially attractive because mechanical properties could then be controlled by biochemical kinetics. One example candidate peptide would be RADSRADC, based on one of the originally synthesized peptides RADn with $n = 8$, 16, 24, or 32. According to some preliminary molecular modeling, the alternating substitution of cysteine for serine does not affect the backbone geometry of the peptide so should not interfere with the self-assembly process.

The cellular solids model has also been used to analyze the elasticity of the intracellular F-actin matrix which exhibits close similarity to our peptide biomaterial in terms of microstructure and dimensions. In that work [9], the value for the elastic modulus predicted by the theory was roughly consistent with independent measurements. It should be noted, though, that while the present results lend some credence to the applicability of the cellular solids model for these materials, this approach neglects Brownian or entropic effects that could be important on these length scales. Indeed, one recent study [17] of tape-like structures ~ 0.7 nm thick and ~ 8 nm wide produced by gelation of a 24-residue oligopeptide used an entropic rubber elasticity model in their interpretation of the observed rheological properties. It is interesting to observe that the elastic modulus of a material characterized by rubber elasticity also exhibits a power law dependence on concentration, to a power of ~ 1.5–2.25 [18].

Acknowledgements

We would like to acknowledge the support of an Engineering/Biology Seed Grant from the MIT Center for Biomedical Engineering.

REFERENCES

1. A. S. Hoffman, *Artificial Organs* **16**, 43 (1992).
2. B. D. Ratner, *J. Biomed. Mat. Res.* **27**, 837 (1993).
3. J. G. Tirrell, M. J. Fournier, T. L. Mason and D. A. Tirrell, *Chem. Eng. News* 40 (19 December 1994).
4. R. Langer, *Ann. Biomed. Eng.* **23**, 101 (1995).
5. S. Zhang, T. Holmes, C. Lockshin and A. Rich, *Proceedings From the National Academy of Science USA* **90**, 3332 (1993).
6. S. Zhang, C. Lockshin, R. Cook and A. Rich, *Biopolymers* **34**, 663 (1994).
7. S. Zhang, T. C. Holmes, C. M. DiPersio, R. O. Hynes, X. Su and A. Rich, *Biomaterials* **16**, 1385 (1995).
8. L. J. Gibson and M. F. Ashby, *Cellular Solids*. Pergamon Press (1988).
9. R. L. Satcher and C. F. Dewey, *Biophys. J.* **71**, 109 (1996).
10. S. P. Timoshenko and J. N. Godier, *Theory of Elasticity*, 3rd edn. McGraw-Hill, New York (1970).
11. D. L. Bader and P. Bowker, *Biomaterials* **11**, 721 (1983).
12. M. Chvapil, *J. Biomed. Mater. Res.* **11**, 721 (1977).
13. M. Chvapil, *J. Biomed. Mater. Res.* **16**, 245 (1982).
14. J. Lawrence-Katz, L. L. Latta, S. Singh and H. S. Yoon, in: *Handbook of Biomedical Engineering*, J. Kline (Ed.), p. 460. Harcourt Brace Jovanovich, New York (1985).
15. K. James and J. Kohn, *MRS Bull.* (20 November 1996).
16. I. Engelberg and J. Kohn, *Biomaterials* **12**, 292 (1991).
17. D. A. Evans, N. J. Beukes and J. L. Kirschvink, *Nature* **386**, 262 (1997).
18. M. Doi and S. E. Edwards, *The Theory of Polymer Dynamics*. Clarendon, Oxford (1961).